Cytoplasmic intermediate filaments mediate actin-driven positioning of the nucleus

Isabelle Dupin, Yasuhisa Sakamoto and Sandrine Etienne-Manneville*

Institut Pasteur, Cell polarity and Migration Group and CNRS URA 2582, 25 rue du Dr Roux, 75724 Paris cedex 15, France

*Author for correspondence (setienne@pasteur.fr)

Accepted 27 October 2010
Journal of Cell Science 124, 865-872

doi:10.1242/jcs.076356

Summary

The localization of the nucleus is precisely regulated, and defects in nuclear positioning are observed in diseases such as lissencephaly, cerebellar ataxia and dysplasia. We show here that cytoplasmic intermediate filaments are essential players in actin-dependent positioning of the nucleus. The actin retrograde flow is relayed by a flow of intermediate filaments that accumulate asymmetrically around the nuclear envelope. Perturbations of the intermediate filament network alter positioning of the nucleus in both migrating and immobile astrocytes. This function of intermediate filaments might be crucial for regulating cell motility, in particular in tumor cells expressing high levels of cytoplasmic intermediate filaments.

Key words: Actin, Intermediate filament, Micropattern, Migration, Nucleus

Introduction

The nucleus is usually positioned at the cell center, but its position can vary depending on the cell type and function. During development, perturbing the anchorage of post-synaptic nuclei in muscular fibers affects the innervation of the muscular cell (Starr, 2007) and leads to respiratory failure and early lethality (Zhang et al., 2007). During cell migration, a forward nucleus translocation is necessary (Tsai and Gleeson, 2005), whereas a rearward movement of the nucleus at the onset of migration participates in fibroblast polarization (Gomes et al., 2005). Nuclear rotations have also been observed in fibroblasts during migration (Levy and Holzbaur, 2008) and in those under mechanical shear stress (Lee et al., 2005). Nucleus mislocalization is routinely used as a clinical marker for disease. A diagnosis for severe epithelial dysplasia is made mainly on the basis of nucleus positioning (Konishi and Morson, 1982). In vitro, nucleus positioning is also dramatically altered in tumor cells (Dupin et al., 2009).

Microtubule and actin cytoskeletal networks have been independently implicated in nuclear movement and anchorage. Microtubules contribute to nucleus forward displacement, either indirectly, by pulling on the centrosome (Tsai and Gleeson, 2005), or directly by forming a cage around the nucleus, which occurs particularly during neuronal migration (Umeshima et al., 2007). Dynein seems to be a key player in anchoring microtubules at the nuclear envelope (Salina et al., 2002) and regulates nucleus position and rotation in migrating cells (Levy and Holzbaur, 2008; Umeshima et al., 2007). The actin cytoskeleton contributes, through actomyosin contractility, to forward nuclear movement in leukocytes (Sanchez-Madrid and del Pozo, 1999) and neuronal cells (Bellion et al., 2005). Moreover, the actin retrograde flow is involved in pushing the nucleus towards the cell rear following wounding of a fibroblast monolayer (Gomes et al., 2005; Luxton et al., 2010). Although some observations suggest that intermediate filaments (IFs) could play a role in regulating nucleus displacement (Gerashchenko et al., 2009; Ralston et al., 2006), the role of the IF cytoskeleton in nucleus positioning remains unclear.

We and others have previously demonstrated that actin, but not the microtubules, is involved in nucleus movement following formation of adherens junction (Desai et al., 2009; Dupin et al., 2009). Here, we show that the actin cytoskeleton controls IF organization around the nucleus and that IFs mediate actin-dependent nucleus positioning.

Results and Discussion

To analyze nucleus positioning, we plated groups of six to eight primary rat astrocytes on 100-μm-diameter circular fibronectin-coated micropatterns. Cells that localized at the edge of the pattern presented anisotropic cellular interactions. Although they were unable to migrate out of the pattern, these cells were polarized towards the free edge of the cell (i.e. the edge not involved in cell–cell contacts) (Dupin et al., 2009). The nucleus was off-centered and localized near to cell–cell contacts (Fig. 1A, +Ca), as shown previously (Dupin et al., 2009). We have also shown previously that the actin cytoskeleton plays a crucial role in regulating nucleus positioning in this assay (see Fig. 3B) (Dupin et al., 2009) and that microtubules are not involved (supplementary material Fig. S1). Nesprins and SUN-domain-containing proteins, which form the 'linkers of the nucleoskeleton to the cytoskeleton' (LINC) complex, have been implicated in linking the actin cytoskeleton to the nuclear envelope and in controlling nucleus positioning in various biological systems (Luxton et al., 2010; Razafsky and Hodzic, 2009). Surprisingly, expression of the nesprin KASH domain, which results in the delocalization of endogenous nesprins (Ketema et al., 2007; Padmakumar et al., 2005), did not affect nucleus off-centering in astrocytes (supplementary material Fig. S2).

To characterize the molecular link between the actin cytoskeleton and the nucleus, we analyzed the organization of the actin cytoskeleton in astrocytes with a centered or an off-centered nucleus. Removal of extracellular Ca^{2+} dissociated cadherin-mediated adherens junctions and, as a consequence, abolished the cell polarity regulated by cell–cell contacts and nucleus off-centering (Dupin et al., 2009). In control cells ('+Ca') and in cells

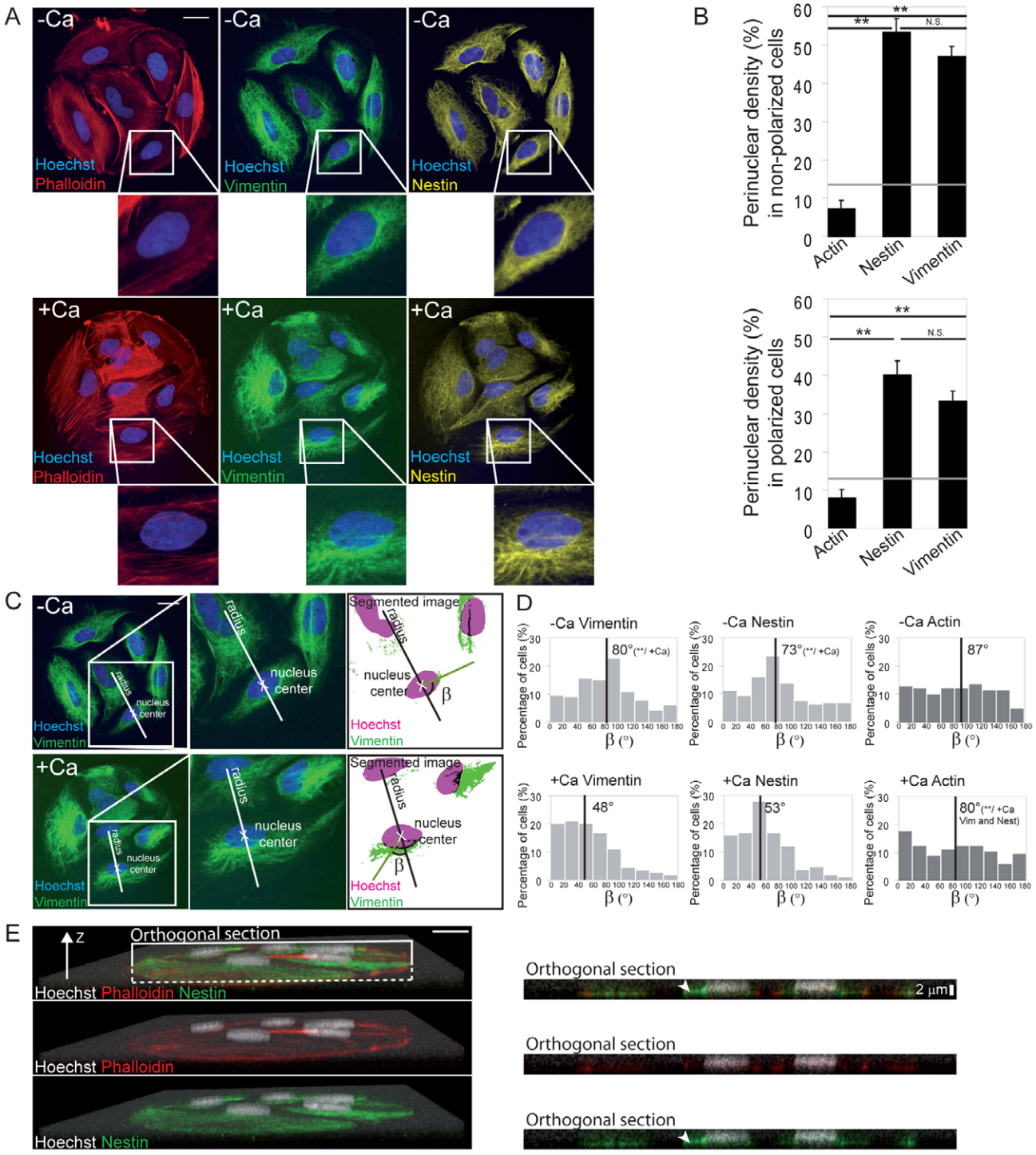

Fig. 1. Cytoplasmic IFs surround the nucleus and accumulate on the side of the nucleus facing the free edge of the cell. Astrocytes were plated onto 100-µm-diameter circular fibronectin-printed micropatterns and fixed 7 hours later. When indicated, the culture medium (+Ca) was changed to Ca^{2+}-free medium 2 hours after plating (–Ca). (**A**,**C**) Hoechst (blue), phalloidin (red), vimentin (green), nestin (yellow) stainings and (**B**) perinuclear density (see supplementary material Fig. S3 for details) of actin, nestin and vimentin. Data are given as means+s.d. for three independent experiments comprising at least 180 cells. **P*<0.05; ***P*<0.005; N.S., not significant. The gray horizontal line indicates the theoretical value (13%) of the perinuclear density in the case of an entirely homogenous staining inside the cell. The right-hand panels in C show segmented images obtained after the image treatment described in supplementary material Fig. S3. 'β' (°) is the angle between the axis defined by the nucleus center and the center of the IF or actin area (green line) and the micropattern radius passing through the nucleus center (black line). (**D**) Distribution of β values. The median angle and statistical differences are indicated in black. ***P*<0.005. (**E**) Hoechst (white), phalloidin (red), nestin (green) stainings. The left-hand panels show three-dimensional reconstructions of the 20 planes acquired with a step of 0.2 µm in the *z*-direction. The right-hand panels show orthogonal sections of the same three-dimensional reconstructions. Scale bars: 20 µm (A, left-hand panels E); 2 µm (right-hand panels E).

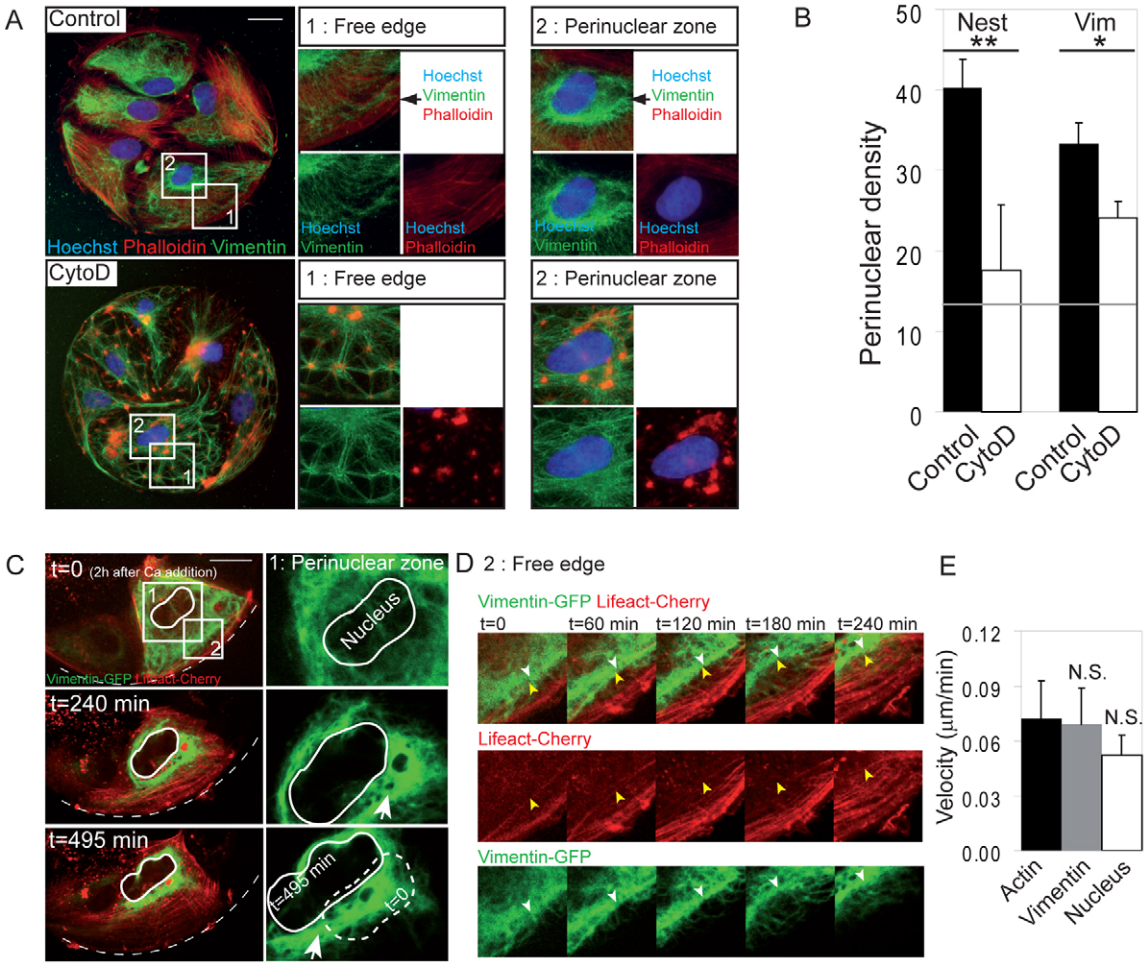

Fig. 2. The actin cytoskeleton controls cytoplasmic IF organization. (**A**,**B**) Primary rat astrocytes were plated onto large fibronectin-printed micropatterns. Cells were treated with 1 µM cytochalasin D (CytoD) 4 hours after plating and fixed 7 hours after plating. (A) Hoechst (blue), phalloidin (red) and vimentin (green) stainings. The middle and right-hand panels show higher magnification of the stainings in the free edge of the cell (1) or in the perinuclear zone (2). (B) Perinuclear density of nestin (Nest) and vimentin (Vim). Data are given as means+s.d. for three independent experiments comprising at least 180 cells. **P*<0.05; ***P*<0.005. The gray horizontal line indicates the theoretical value (13%) of the perinuclear density in the case of an entirely homogenous staining inside the cell. (**C**–**E**) Astrocytes transiently coexpressing EGFP–vimentin and LifeAct–Cherry were left to adhere onto adhesive micropatterns for 2 hours in Ca^{2+}-containing medium, which was then exchanged for Ca^{2+}-free medium for a further 2 hours. Ca^{2+} was then added back into the medium, to promote adherens junction formation and nuclear movement. The cell was imaged every 15 minutes from 2 hours after the Ca^{2+} re-addition (*t*=0). (C) Selected images, at the indicated times, from supplementary material Movie 2. The right-hand panels show a higher magnification of the GFP image in the perinuclear region. The nucleus shape is highlighted by a continuous white line. At *t*=495 minutes, the initial position of the nucleus (broken line) is also shown. White arrows point to the perinuclear IF accumulation. (D) High-magnification image of the free edge of the cell upon Ca^{2+} addition, showing vimentin filaments (white arrowheads) moving together with actin fibers (yellow arrowheads). (E) Velocities of actin, vimentin filaments and the nucleus measured in six cells during the Ca^{2+} switch experiment. **P*<0.05; N.S., not significant. Scale bars: 20 µm.

in Ca^{2+}-free medium ('–Ca'), the perinuclear area was relatively devoid of actin filaments (Fig. 1A). We found that IFs, by contrast, were concentrated around the nucleus (Fig. 1A). Perinuclear density (see supplementary material Fig. S3 for a description of how this is calculated) of the nestin and vimentin IF proteins (Eliasson et al., 1999) was very high, whereas there was a low perinuclear density of actin filaments (Fig. 1B).

To determine whether the IF distribution around the nucleus was homogenous or polarized, we measured the angle 'β' between the axis defined by the nucleus center and the center of the IF area and that of the radius of the micropattern passing through the nucleus center (Fig. 1C; see the Materials and Methods section). For an accumulation of IFs on the side of the nucleus facing the free edge of the cell, this angle is 0°, whereas a homogenous accumulation of IFs around an elliptic nucleus leads to a distribution that peaks around a median value of 90°. The latter type of distribution was observed in non-polarized cells as the median angle was close to 90° (Fig. 1D, –Ca). By contrast, in polarized cells, the distribution of the angles was shifted towards lower values, indicating a preferential recruitment of vimentin and nestin fibers on the side of the nucleus facing the free edge of the cell, whereas the distribution of the angles for the actin cytoskeleton was uniform (Fig. 1D, +Ca). Stronger accumulation of IFs on the side of the nucleus facing the free edge of the cell was also observed in three-dimensional reconstructions of the cells (Fig. 1E, arrowheads). Interestingly, perturbation of the actin cytoskeleton by cytochalasin D treatment dramatically perturbed the organization of IFs and prevented IF accumulation around the nucleus (Fig.

2A,B; supplementary material Movie 1). Moreover, downregulation of lamin B1 (but not lamin A), a major component of the intranuclear IFs that cover the internal surface of the nuclear envelope, inhibited the polarized accumulation of vimentin and nestin (supplementary material Fig. S4A–C), suggesting that IFs interact with the nuclear envelope.

Astrocytes transiently coexpressing EGFP–vimentin and LifeAct–Cherry, a peptide that stains F-actin (Riedl et al., 2008), were imaged during Ca^{2+}-induced nuclear movement (Fig. 2C; supplementary material Movie 2). Addition of Ca^{2+} induced a flow of actin fibers from the free edge of the cell, which was paralleled by a flow of IFs towards the nucleus (Fig. 2D). Vimentin and actin filaments moved at the same velocity (0.07 μm/minute) (Fig. 2E). Small interfering RNA (siRNA)-induced depletion of plectin, a protein able to act as a bridge between actin filaments and IFs, neither prevented actin-driven reorganization of IFs (data not shown) nor altered nucleus localization (supplementary material Fig. S5). Vimentin accumulation on the side of the nucleus facing the free edge of the cell coincided with nuclear displacement (Fig. 2C,D).

The fact that IFs accumulate around the nuclear envelope, following actin rearrangements, led us to investigate whether IFs were involved in actin-dependent nucleus positioning. We generated specific siRNAs targeting nestin, vimentin and glial fibrillary acidic protein (GFAP) which we used for single, double or triple depletion of the major IF proteins in astrocytes (Eliasson et al., 1999). All siRNAs led to a strong decrease (at least 89% for each single depletion) in the corresponding protein expression (supplementary material Fig. S6). Depletion of IF proteins strongly perturbed nucleus off-centering, without significantly affecting actin structures (Fig. 3A,B). We analyzed the dynamics of actin structures in IF-depleted astrocytes expressing LifeAct–Cherry. IF protein depletion inhibited nuclear translocation without perturbing the retrograde flow of actin fibers, which, under these conditions, moved under or above the nucleus with a velocity comparable to that in control cells (Fig. 3C–E; supplementary material Movie 3). Finally, to check that the IF depletion was not affecting nucleus positioning by modifying cytoskeletal tension, we used siRNA to inhibit the expression of myosin IIA and IIB. Myosin II depletion did not perturb nucleus positioning, showing that actomyosin contractility was not involved in the regulation of nucleus positioning (supplementary material Fig. S7). The fact that nucleus off-centering was not totally abolished following transfection of siRNA against all three IF proteins might be due to the remaining expression of IF proteins in these conditions (supplementary material Fig. S6) or might suggest that there is an alternative mechanism that controls nucleus positioning. We excluded any involvement of microtubules by combining IF depletion with nocodazole treatment, which does not induce further defects in nucleus localization (supplementary material Fig. S1D).

We confirmed the important role of the IF network in nucleus positioning by using a dominant-negative GFAP construct (Fig. 3B), corresponding to the N-terminal fragment of GFAP (i.e. lacking the tail region and a part of the rod domain), which is known to perturb the entire IF network, as described with the equivalent vimentin construct (Whipple et al., 2008). Interestingly, depletion of lamin B1 also altered nucleus positioning (supplementary material Fig. S4D,E).

The role of IFs in actin-dependent nucleus positioning was further confirmed by plating single astrocytes on crossbow-shaped micropatterns; on these micropatterns nucleus position is determined by the geometry of cell interactions with the extracellular matrix, with the nucleus preferentially localizing near the non-adhesive region of the cells (Dupin et al., 2009; Thery et al., 2006) (Fig. 3F–J). To determine whether the role of IFs in nucleus positioning was cell-type specific, we analyzed nucleus positioning in human adrenal carcinoma SW13 cells, either expressing or not expressing vimentin, and mouse embryonic fibroblasts (MEFs) from wild-type and vimentin-knockout mice. In both cell types, nucleus off-centering was strongly dependent on the expression of vimentin, indicating that IFs might control nucleus positioning in a large variety of cell types (Fig. 3J). Taken together, these results indicate that, in addition to the actin cytoskeleton, IFs play a fundamental role in nuclear localization downstream of both intercellular contacts and cellular interactions with the extracellular matrix. These results lead us to propose that the retrograde flow of actin can control nucleus movement by promoting the polarized perinuclear accumulation of cytoplasmic IFs, which, in turn, push against the nuclear envelope to move it across the cytoplasm (supplementary material Fig. S8). As inhibition of nesprin or depletion of plectin does not affect nucleus positioning (supplementary material Figs S2 and S5), the LINC complex does not seem to be involved in the connection between cytoplasmic IFs and the nucleus, suggesting the existence of an alternative connection. As nestin and vimentin are present inside the nucleus (Spencer et al., 2000; Thomas et al., 2004; Veselska et al., 2006), and vimentin directly interacts with lamin B but not lamin A (Georgatos and Blobel, 1987), IFs might directly interact with the lamina. This would be consistent with our results showing that nucleus positioning and the polarized perinuclear accumulation of IFs depend on lamin B1 but not lamin A (supplementary material Fig. S4). Alternatively, we cannot exclude the possibility that IFs act by physically pushing against the nucleus without being directly coupled to the nuclear envelope.

We next determined whether IFs also play a role in nucleus positioning during wound-induced astrocyte migration. Nucleus localization at the rear of the IF-depleted migrating cells was less pronounced than in control cells (Fig. 4A,B) (Dupin et al., 2009; Gomes et al., 2005). We followed the nucleus center and a nucleolus to measure the nuclear angular velocity (Fig. 4C,D). Nuclear rotations (Levy and Holzbaur, 2008) were strongly inhibited in IF-depleted cells (Fig. 4C,D; supplementary material Movies 4 and 5), suggesting that, in addition to microtubules, IFs affect nuclear rotation (Lee et al., 2005). We also found that nuclear velocity was reduced and the nuclear movement was less directed compared with that in control cells (Fig. 4E,F). As previously reported (Lepekhin et al., 2001), simultaneous depletion of nestin, vimentin and GFAP eventually led to a delay in wound closure (Fig. 4G,H), which could be a consequence or a cause of the reduced and less-directed nucleokinesis. IF depletion also perturbed the orientation of the nucleus–centrosome axis in immobile and motile astrocytes (supplementary material Fig. S9A,B). Interestingly, and in contrast with nucleus positioning, centrosome positioning was mainly dependent on nestin but not on GFAP and vimentin (supplementary material Fig. S9C), suggesting that control of centrosome positioning by nestin is not related to the regulation of nucleus positioning by IFs.

Our observations corroborate reports on IF-null mouse models, where the formation of the glial scar by astrocytes after brain injury is impaired (Pekny et al., 1999). Conversely, increased expression of nestin and vimentin has been associated with elevated invasiveness and malignancy in astrocytomas (Dahlstrand et al.,

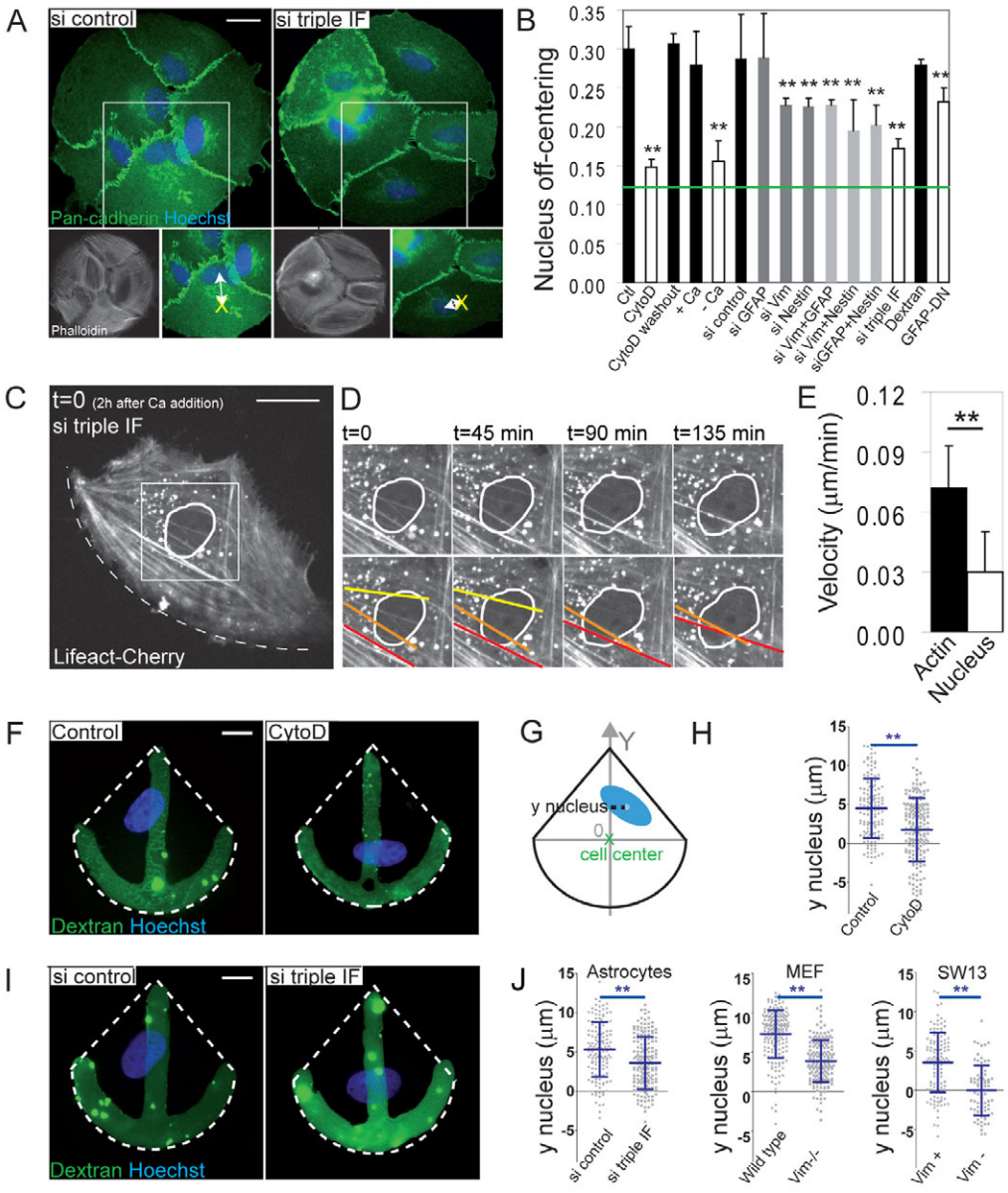

Fig. 3. IFs control nucleus position in several cell types. Three days following nucleofection of the indicated siRNAs, astrocytes [or for panel J, SW13 cells expressing (Vim +) or not expressing (Vim –) vimentin, and wild-type MEFs or MEFs from vimentin-knockout mice (Vim–/–)] were plated onto 100-µm-diameter circular micropatterns (A,B) or crossbow-shaped micropatterns (F–J). Astrocytes were incubated for 2 hours in the presence of Ca^{2+}. Cells were either incubated in Ca^{2+}-free medium (–Ca) for 7 hours or incubated for 2 hours in Ca^{2+}-free medium followed by 7 hours in Ca^{2+}-containing medium (+Ca). When indicated, cells were treated, 4 h after plating, with 1 µM cytochalasin D; cytochalasin-D-treated cells were fixed after 3 hours (CytoD), or further incubated for 5 hours in normal medium (CytoD washout). Alternatively, cells were micro-injected 2 hours after plating with dextran, or with dextran and a dominant-negative GFAP construct (GFAP-DN) and incubated for 5 hours. 'si triple IF' indicates the triple depletion of vimentin, GFAP and nestin by siRNA. (**A**) Cells were fixed and stained for pan-cadherin (green) and with Hoechst (blue). The lower-left-hand panels show phalloidin staining and the lower-right-hand panels a higher magnification of a typical cell with the cell center indicated (yellow cross). (**B**) Nucleus off-centering, defined as the distance between the nucleus center and the cell centroid divided by the square root of the cell area. The green horizontal line indicates the off-centering value (0.12) in single cells plated onto a symmetrical micropattern. Data are given as means+s.d. of three independent experiments totalizing at least 180 cells; statistical differences between the gray or white bars and the corresponding control black bar on their left (Ctl) are indicated. $^{**}P<0.005$. (**C**–**E**) IF-depleted astrocytes (si triple IF) transiently expressing LifeAct–Cherry were left to adhere onto adhesive micropatterns for 2 hours in the presence of Ca^{2+}, the medium was then exchanged for Ca^{2+}-free medium for 2 hours. Ca^{2+} was then added back to the medium and, after a further 2 hours (t=0), the cell was imaged every 15 minutes. (C) Selected image, at t=0, from supplementary material Movie 3. The nucleus shape is highlighted by a white line. (D) Higher magnification of the perinuclear region upon Ca^{2+} addition showing actin fibers (red, orange and yellow) moving in various directions above or under the nucleus. (E) Velocities of actin filaments and the nucleus measured in six IF-depleted cells during the Ca^{2+} switch experiment. $^{**}P<0.005$. (**F**,**I**) Dextran fluorescence (green) and Hoechst staining (blue) showing the micropattern and the nucleus. (**G**) Schematic defining the 'y nucleus' distance (µm) between the nucleus center (blue dot) and the cell center (green cross) along the symmetry axis (Y axis) of the pattern. (**H**,**J**) y nucleus position (gray spots) measured on at least 78 cells of the indicated cell types. The blue horizontal line and vertical bar indicate means±s.d. Statistical differences are indicated. $^{**}P<0.005$. Scale bars: 20 µm (A,C); 10 µm (F,I).

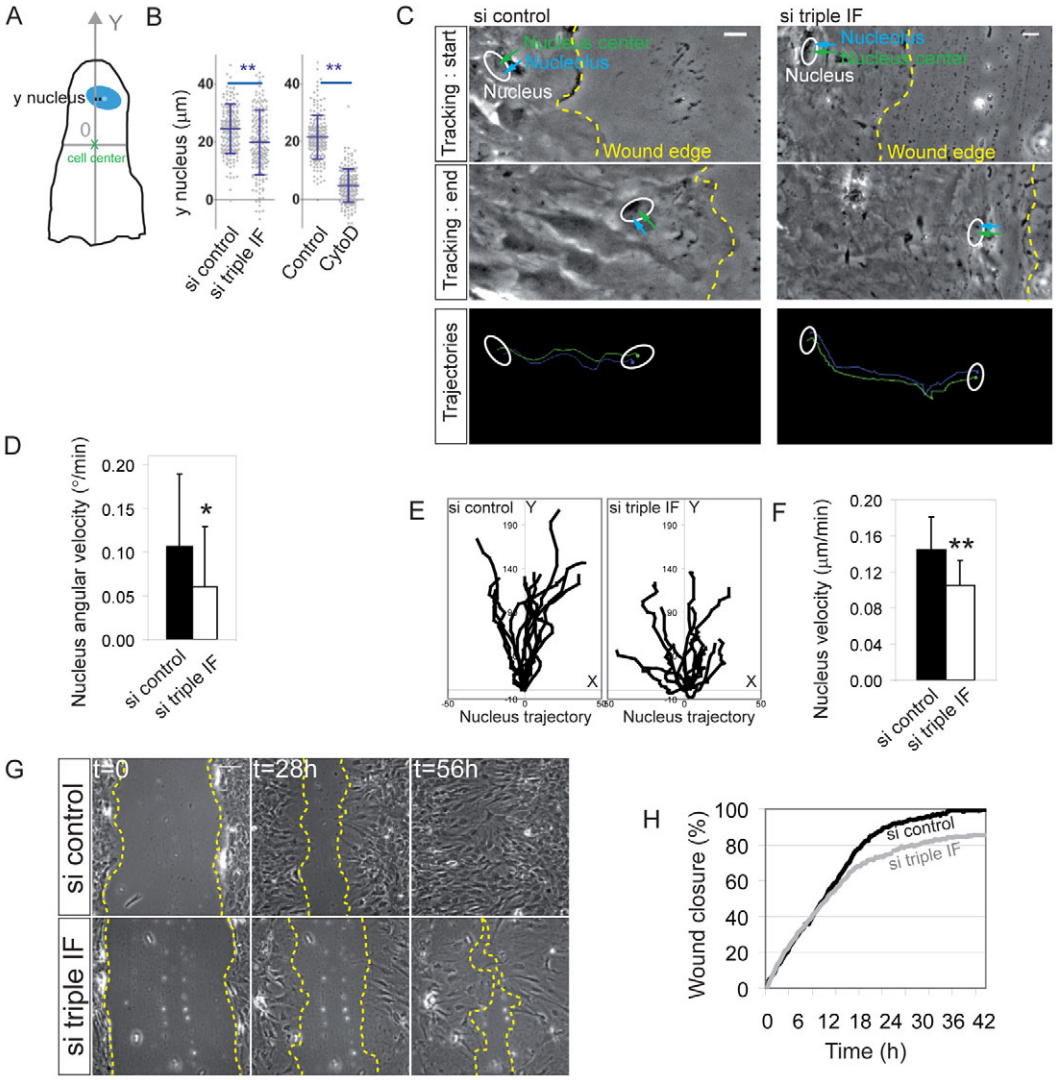

Fig. 4. Depletion of IFs alters nucleus positioning and nucleus rotation during migration. Primary rat astrocytes were nucleofected with control or IF-directed siRNA or pretreated with cytochalasin D (0.5 µM, 1 hour). (**A**) Schematic defining the 'y nucleus' distance (µm) between the nucleus center (blue dot) and the cell center (green cross) along the direction perpendicular to the wound (Y axis). (**B**) y nucleus position (gray spots) measured in 180 cells at 7 hours after wounding. The blue horizontal line and vertical bar indicate mean±s.d. Statistical differences between control cells and IF-depleted cells or between control and cytochalasin-D -treated cells are indicated. $^{**}P<0.005$. (**C**) Selected phase-contrast images from supplementary material Movies 4 and 5. First and last tracked images, and the trajectories of a nucleolus (blue line) and the nucleus center (green line) are shown. Nucleus borders (white oval), nucleoli (blue arrow), nucleus center (green arrow) and wound edges (broken yellow line) are shown. (**D**) Nucleus angular velocity [degrees (°) per minute]. Data are means±s.d. of the velocities measured on at least 25 cells. $^{*}P<0.05$. (**E**) A total of 13 typical nucleus trajectories in cells tracked for a period of 10 hours. The 'Y axis' indicates the direction perpendicular to the wound. (**F**) Nucleus velocity (µm/minute). Data are means±s.d. of the velocities measured in at least 25 cells. $^{**}P<0.005$. (**G**) Phase-contrast images from a wound-healing assay taken immediately after wounding (t=0), and at 28 hours and 56 hours after wounding. The wound edge is indicated by a broken yellow line. (**H**) Wound closure, defined as the ratio between the space filled by cells and the free space at t=0. Data are the mean of three independent experiments. Scale bars: 20 µm (C); 100 µm (G).

1992; Rutka et al., 1999). As the expression pattern of IFs is regulated during cell differentiation (Fuchs and Weber, 1994), this study provides new insights on the mechanisms of nucleus positioning not only in diseases but also during development.

Materials and Methods

Materials

We used primary antibodies against the following proteins: pan-cadherin CH-19 (Sigma), GFAP, vimentin, lamin A (Santa Cruz Biotechnology), nestin (Chemicon), pericentrin, nesprin-1α, myosin IIA, myosin IIB (Covance), plectin, lamin B1 (Abcam) and α-tubulin (AbD Serotec). Cytochalasin D and nocodazole were from Sigma. TRITC-conjugated secondary antibodies were from Jackson Immunoresearch); Alexa-Fluor-488-conjugated secondary antibodies and rhodamine–phalloidin were from Invitrogen. pLifeact-Cherry was a gift from Matthieu Piel (Institut Curie, Paris, France) (Riedl et al., 2008) and pVimentin–GFP was a gift from Danielle Pham-Dinh (INSERM UMR 546, Paris, France) (Mignot et al., 2007). siRNA duplexes corresponding to rat GFAP starting at nucleotide 757 (GenBank accession no. NM_017009), rat vimentin starting at 781 (GenBank accession no. NM_031140), rat nestin starting at 780 (GenBank accession no. NM_012987), rat plectin starting at 5727 and 6128 (GenBank accession no. NM_0224010), rat lamin A starting at 648 and 810 (GenBank accession no. BC062018), rat lamin B1 starting at 625 and 1262 (GenBank accession no. NM_053905), rat myosin IIA starting at 1853 (GenBank accession no. NM_013194, rat myosin IIB starting at 506 (GenBank accession no. NM_031520) were obtained from Proligo. For the dominant-negative GFAP construct, GFAP cDNA encoding 1– 595 bp was inserted into pCMV-FLAG in the *Eco*RI/*Bgl*II site. pCMV SPORT6-mouse Syne 1 (nesprin-1α) was purchased from Geneservice. Nesprin-1α was amplified by PCR using primers forward

5′-GCCGCTCGAGCGGTGGTGGCAGAGGACTTGCATGGCCCG-3′ and reverse 5′-CGCCGGAATTCCGTCAGAGTGGAGGAGGACCGTTGGTATATCT-3′, and the resulting fragment was subcloned into pEGFP-C1 in the *Xho*/*Eco*RI site. The last 1035 bp of nesprin-1α, corresponding to the KASH domain, was inserted into pRK5-MYC in the *Bgl*II/*Eco*RI site by subcloning using primers forward 5′-GCGGAAGATCTTCCGCCTGGCTAGGAGAGACAGAGGAGGAG-3′ and reverse 5′-CGCCGGAATTCCGTCAGAGTGGAGGAGGACCGTTGGTATATCT-3′. siRNA and DNA constructs were introduced into cells using nucleofection technology (Amaxa) (Etienne-Manneville et al., 2005). Nuclear microinjections were performed using expression vectors at 100 μg/ml.

Stamp fabrication, micro-contact printing and cell plating

Moulds for stamps were obtained from Biotray (ENS, Lyon). Stamp fabrication and micro-contact printing were performed as described previously (Dupin et al., 2009). Briefly, PDMS stamps were coated with fibronectin (0.005%). After printing, glass coverslips were then treated with poly-lysine-grafted-poly(ethylene glycol), to prevent cells spreading outside of the patterns. Culture of primary astrocytes was as described previously (Etienne-Manneville, 2006; Etienne-Manneville and Hall, 2001). SW13 cells not expressing vimentin were a gift from Zhigang Xue (UR4, UPMC, Paris, France). SW13 cells expressing vimentin and vimentin double-knockout MEFs (Colucci-Guyon et al., 1994) were gifts from Bertrand Favre (Department of Dermatology, University Hospital, Geneva, Switzerland) and Harald Herrmann (Department of Molecular Genetics, German Cancer Research Center, Heidelberg, Germany), respectively. Wild-type MEFs were a gift from Hélène Saklani (Institut Pasteur, Paris, France). Cells were trypsinized and agitated for 30 minutes at 37°C in 0.5% fetal calf serum (FCS)-containing medium, deposited onto the printed coverslip and centrifuged at 800 ***g*** for 5 minutes. For the Ca^{2+} switch experiments, the medium was changed 2 hours after centrifugation for a Ca^{2+}-depleted medium (Invitrogen) supplemented with 0.5% FCS. After a further 2 hours, Ca^{2+} was added back into the medium at a final concentration of 1.8 mM.

Image acquisition and analysis, and statistical analysis

Fixed cells were imaged on a microscope (DM6000B; Leica) using an HCX plan Apo 40×/1.25 NA oil CS or HCX plan Apo 63×/1.40 NA oil CS objective (Leica). For *z*-stacks, fixed cells were imaged on a confocal (TCS SP5; Leica) microscope (DM6000B, Leica) using a HCX plan Apo 63×/1.40 NA oil CS objective (Leica). Three-dimensional reconstructions and orthogonal sections were made using Imaris software. For time-lapse microscopy, astrocytes were imaged at 37°C with a plan Apo 63×/1.40 NA oil objective (supplementary material Movies 1–3) on a spinning-disk confocal microscope (Axiovert 200, Zeiss) with an N plan 10×/0.25 NA dry objective (Leica) on a microscope (DMI6000B, Leica) (supplementary material Movies 4 and 5). The imaging medium was Dulbecco's modified Eagle's medium (DMEM) without Phenol Red (Invitrogen), supplemented with 0.5% FCS (supplementary material Movies 1–3) or normal medium (supplementary material Movies 4 and 5). Cells in supplementary material movies 1-3 were imaged with a planApo 63×/1.40 NA oil objective on a spinning-disk confocal microscope (Axiovert 200, Zeiss). Cells in supplementary material movies 4 and 5 were imaged with an N plan 10×/0.25 NA dry objective (Leica) on a microscope (DMI6000B, Leica). Microscopes were equipped with a camera (C9100, Zeiss) (DFC350 FX, Leica) and images were collected with the Volocity software (Zeiss) or the LAS software (Leica). Image analysis and measurements were performed with the ImageJ software. Image analysis was always performed on non-modified images. For figures, brightness and contrast were adjusted. The contrast of supplementary material Movie 2 was enhanced by equalizing the histogram with the ImageJ software. The perinuclear density of proteins was calculated as described in supplementary material Fig. S3. Briefly, a binary threshold is applied to the Hoechst image to select the nucleus. The perinuclear area is defined as an area of a 2-μm greater radius than the nucleus area. On IF or actin images, background-subtracted fluorescence intensity was normalized to the highest intensity of that image as described previously (Webb et al., 2004). The perinuclear density (percentage) is defined by the ratio between the area of segmented pixels in the perinuclear area and the total area of segmented pixels divided by the number of cells. Angle β (°) is the angle between the axis passing through the nucleus center and the segmented area center for IFs and the radius of the micropattern passing through the nucleus center (Fig. 1): for an accumulation of IFs on the side of the nucleus facing the free edge of the cell this angle is 0°; for a randomly oriented accumulation around the nucleus this angle can take any value between 0 and 180°, giving a median value of 90° for a population of cells with a randomly oriented accumulation. The velocities of actin, vimentin filaments and nuclei were calculated using the Manual Tracking plugin of the ImageJ software (supplementary material Movies 2 and 3). To record the positions of the nucleus and pattern centroid, a threshold value of fluorescence intensity was chosen to select the nucleus or the pattern from the appropriate images, respectively. The cell contour was manually determined using images of the cadherin staining, or dextran fluorescence for micro-injected cells, and the cell area was then calculated. The coordinates of the centroid of thresholded or selected objects was measured. The distances from the nucleus centroid to the cell centroid were calculated. 'Nucleus off-centering' was defined as the distance between the nucleus and cell centroid divided by the square root of cell area (Fig. 3; supplementary material Figs S1, S2, S4, S5 and S7). Nuclear angular velocity is described as the angle between the axis passing through the nucleus center and a nucleolus at the beginning of the tracking and the same axis at the end of the tracking, divided by the tracking time (Fig. 4C,D). For migrating cells, cell orientation was analyzed by measuring the angle 'α' between the centrosome–nucleus axis and an axis perpendicular to the wound (supplementary material Fig. S9). For a polarized cell oriented towards the free edge of the pattern (immobile cells) or towards the wound (migrating cells) this angle is 0° (see supplementary material Fig. S9). For a randomly oriented cell, this angle can take any value between 0 and 180°, giving a median value of 90° for a population of randomly oriented cells.

Statistical differences were determined using Student's *t*-tests (for nucleus position, velocity and perinuclear density comparison) or the Wilcoxon test (for angle distribution comparison) (Prism 5.0, GraphPad Software, CA). Statistical significance is defined as $P<0.05$.

We thank Danielle Pham-Dinh for vimentin and GFAP constructs, Matthieu Piel for the pLifeact-Cherry plasmid, Zhigang Xue for vimentin^{-} SW13 cells, Bertrand Favre and Harald Herrmann for vimentin^{+} SW13 cells and vimentin$^{-/-}$ MEFs, Hélène Saklani (Institut Pasteur, Paris, France) for wild-type MEFs and the Plateforme d'Imagerie Dynamique of the Institut Pasteur for technical support. I.D. is funded by the Ministère de la Recherche and the Fondation pour la Recherche Médicale and Y.S. by the Uehara memorial foundation. This work was supported by the Institut Pasteur, the Agence Nationale pour la Recherche and by La Ligue contre le Cancer. S.E.-M. is a member of the EMBO YIP.

Supplementary material available online at
http://jcs.biologists.org/cgi/content/full/124/6/865/DC1

References

Bellion, A., Baudoin, J. P., Alvarez, C., Bornens, M. and Metin, C. (2005). Nucleokinesis in tangentially migrating neurons comprises two alternating phases: forward migration of the Golgi/centrosome associated with centrosome splitting and myosin contraction at the rear. *J. Neurosci.* **25**, 5691-5699.

Colucci-Guyon, E., Portier, M. M., Dunia, I., Paulin, D., Pournin, S. and Babinet, C. (1994). Mice lacking vimentin develop and reproduce without an obvious phenotype. *Cell* **79**, 679-694.

Dahlstrand, J., Collins, V. P. and Lendahl, U. (1992). Expression of the class VI intermediate filament nestin in human central nervous system tumors. *Cancer Res.* **52**, 5334-5341.

Desai, R. A., Gao, L., Raghavan, S., Liu, W. F. and Chen, C. S. (2009). Cell polarity triggered by cell-cell adhesion via E-cadherin. *J. Cell Sci.* **22**, 905-911.

Dupin, I., Camand, E. and Etienne-Manneville, S. (2009). Classical cadherins control nucleus and centrosome position and cell polarity. *J. Cell Biol.* **185**, 779-786.

Eliasson, C., Sahlgren, C., Berthold, C. H., Stakeberg, J., Celis, J. E., Betsholtz, C., Eriksson, J. E. and Pekny, M. (1999). Intermediate filament protein partnership in astrocytes. *J. Biol. Chem.* **274**, 23996-24006.

Etienne-Manneville, S. (2006). In vitro assay of primary astrocyte migration as a tool to study Rho GTPase function in cell polarization. *Methods Enzymol.* **406**, 565-578.

Etienne-Manneville, S. and Hall, A. (2001). Integrin-mediated activation of Cdc42 controls cell polarity in migrating astrocytes through PKCzeta. *Cell* **106**, 489-498.

Etienne-Manneville, S., Manneville, J. B., Nicholls, S., Ferenczi, M. A. and Hall, A. (2005). Cdc42 and Par6-PKCzeta regulate the spatially localized association of Dlg1 and APC to control cell polarization. *J. Cell Biol.* **170**, 895-901.

Fuchs, E. and Weber, K. (1994). Intermediate filaments: structure, dynamics, function, and disease. *Annu. Rev. Biochem.* **63**, 345-382.

Georgatos, S. D. and Blobel, G. (1987). Lamin B constitutes an intermediate filament attachment site at the nuclear envelope. *J. Cell Biol.* **105**, 117-125.

Gerashchenko, M. V., Chernoivanenko, I. S., Moldaver, M. V. and Minin, A. A. (2009). Dynein is a motor for nuclear rotation while vimentin IFs is a "brake". *Cell Biol. Int.* **33**, 1057-1064.

Gomes, E. R., Jani, S. and Gundersen, G. G. (2005). Nuclear movement regulated by Cdc42, MRCK, myosin, and actin flow establishes MTOC polarization in migrating cells. *Cell* **121**, 451-463.

Ketema, M., Wilhelmsen, K., Kuikman, I., Janssen, H., Hodzic, D. and Sonnenberg, A. (2007). Requirements for the localization of nesprin-3 at the nuclear envelope and its interaction with plectin. *J. Cell Sci.* **120**, 3384-3394.

Konishi, F. and Morson, B. C. (1982). Pathology of colorectal adenomas: a colonoscopic survey. *J. Clin. Pathol.* **35**, 830-841.

Lee, J. S., Chang, M. I., Tseng, Y. and Wirtz, D. (2005). Cdc42 mediates nucleus movement and MTOC polarization in Swiss 3T3 fibroblasts under mechanical shear stress. *Mol. Biol. Cell* **16**, 871-880.

Lepekhin, E. A., Eliasson, C., Berthold, C. H., Berezin, V., Bock, E. and Pekny, M. (2001). Intermediate filaments regulate astrocyte motility. *J. Neurochem.* **79**, 617-625.

Levy, J. R. and Holzbaur, E. L. (2008). Dynein drives nuclear rotation during forward progression of motile fibroblasts. *J. Cell Sci.* **121**, 3187-3195.

Luxton, G. W., Gomes, E. R., Folker, E. S., Vintinner, E. and Gundersen, G. G. (2010). Linear arrays of nuclear envelope proteins harness retrograde actin flow for nuclear movement. *Science* **329**, 956-959.

Mignot, C., Delarasse, C., Escaich, S., Della Gaspera, B., Noe, E., Colucci-Guyon, E., Babinet, C., Pekny, M., Vicart, P., Boespflug-Tanguy, O. et al. (2007). Dynamics of mutated GFAP aggregates revealed by real-time imaging of an astrocyte model of Alexander disease. *Exp. Cell Res.* **313**, 2766-2779.

Padmakumar, V. C., Libotte, T., Lu, W., Zaim, H., Abraham, S., Noegel, A. A., Gotzmann, J., Foisner, R. and Karakesisoglou, I. (2005). The inner nuclear membrane protein Sun1 mediates the anchorage of Nesprin-2 to the nuclear envelope. *J. Cell Sci.* **118**, 3419-3430.

Pekny, M., Johansson, C. B., Eliasson, C., Stakeberg, J., Wallen, A., Perlmann, T., Lendahl, U., Betsholtz, C., Berthold, C. H. and Frisen, J. (1999). Abnormal reaction to central nervous system injury in mice lacking glial fibrillary acidic protein and vimentin. *J. Cell Biol.* **145**, 503-514.

Ralston, E., Lu, Z., Biscocho, N., Soumaka, E., Mavroidis, M., Prats, C., Lomo, T., Capetanaki, Y. and Ploug, T. (2006). Blood vessels and desmin control the positioning of nuclei in skeletal muscle fibers. *J. Cell. Physiol.* **209**, 874-882.

Razafsky, D. and Hodzic, D. (2009). Bringing KASH under the SUN: the many faces of nucleo-cytoskeletal connections. *J. Cell Biol.* **186**, 461-472.

Riedl, J., Crevenna, A. H., Kessenbrock, K., Yu, J. H., Neukirchen, D., Bista, M., Bradke, F., Jenne, D., Holak, T. A., Werb, Z. et al. (2008). Lifeact: a versatile marker to visualize F-actin. *Nat. Methods*. **5**, 605-607.

Rutka, J. T., Ivanchuk, S., Mondal, S., Taylor, M., Sakai, K., Dirks, P., Jun, P., Jung, S., Becker, L. E. and Ackerley, C. (1999). Co-expression of nestin and vimentin intermediate filaments in invasive human astrocytoma cells. *Int. J. Dev. Neurosci.* **17**, 503-515.

Salina, D., Bodoor, K., Eckley, D. M., Schroer, T. A., Rattner, J. B. and Burke, B. (2002). Cytoplasmic dynein as a facilitator of nuclear envelope breakdown. *Cell* **108**, 97-107.

Sanchez-Madrid, F. and del Pozo, M. A. (1999). Leukocyte polarization in cell migration and immune interactions. *EMBO J.* **18**, 501-511.

Spencer, V. A., Samuel, S. K. and Davie, J. R. (2000). Nuclear matrix proteins associated with DNA in situ in hormone-dependent and hormone-independent human breast cancer cell lines. *Cancer Res.* **60**, 288-292.

Starr, D. A. (2007). Communication between the cytoskeleton and the nuclear envelope to position the nucleus. *Mol. Biosyst.* **3**, 583-589.

Thery, M., Racine, V., Piel, M., Pepin, A., Dimitrov, A., Chen, Y., Sibarita, J. B. and Bornens, M. (2006). From the Cover: Anisotropy of cell adhesive microenvironment governs cell internal organization and orientation of polarity. *Proc. Natl. Acad. Sci. USA* **103**, 19771-19776.

Thomas, S. K., Messam, C. A., Spengler, B. A., Biedler, J. L. and Ross, R. A. (2004). Nestin is a potential mediator of malignancy in human neuroblastoma cells. *J. Biol. Chem.* **279**, 27994-27999.

Tsai, L. H. and Gleeson, J. G. (2005). Nucleokinesis in neuronal migration. *Neuron* **46**, 383-388.

Umeshima, H., Hirano, T. and Kengaku, M. (2007). Microtubule-based nuclear movement occurs independently of centrosome positioning in migrating neurons. *Proc. Natl. Acad. Sci. USA* **104**, 16182-16187.

Veselska, R., Kuglik, P., Cejpek, P., Svachova, H., Neradil, J., Loja, T. and Relichova, J. (2006). Nestin expression in the cell lines derived from glioblastoma multiforme. *BMC Cancer* **6**, 32.

Webb, D. J., Donais, K., Whitmore, L. A., Thomas, S. M., Turner, C. E., Parsons, J. T. and Horwitz, A. F. (2004). FAK-Src signalling through paxillin, ERK and MLCK regulates adhesion disassembly. *Nat. Cell Biol.* **6**, 154-161.

Whipple, R. A., Balzer, E. M., Cho, E. H., Matrone, M. A., Yoon, J. R. and Martin, S. S. (2008). Vimentin filaments support extension of tubulin-based microtentacles in detached breast tumor cells. *Cancer Res.* **68**, 5678-5688.

Zhang, X., Xu, R., Zhu, B., Yang, X., Ding, X., Duan, S., Xu, T., Zhuang, Y. and Han, M. (2007). Syne-1 and Syne-2 play crucial roles in myonuclear anchorage and motor neuron innervation. *Development* **134**, 901-908.